ISSN 1560-0904, Polymer Science, Series B, 2021, Vol. 63, No. 6, pp. 790–801. © Pleiades Publishing, Ltd., 2021.

FUNCTIONAL POLYMERS

Thermally Conductive Composites Obtained by Carbon Nanotubes Filling Immiscible Polyamide 6/Poly (phenylene sulfide) Blends

Yi Lin[a], Feng Lang[a], Dan Zeng[a], Duxin Li[a,*], Chunguang Xiao[a], Yu Xiang[a], and Jinfei Shangguan[a]

[a]*State Key Laboratory for Powder Metallurgy, Central South University, Changsha, 410083 China*

**e-mail: liduxin6404@csu.edu.cn*

Received March 18, 2021; revised August 15, 2021; accepted September 3, 2021

Abstract—Polyamide-type composites with improved thermal conductivity are prepared by using polyamide 6(PA6)/poly (phenylene sulfide)(PPS) 6 : 4 blend as the matrix and carbon nanotubes (MWCNTs) as the filler through melt compounding. Blends of MWCNTs/PPS/PA6 were melt blended with two different mixing sequences. At the MWCNTs loading of 8.69 wt %, thermal conductivity of MWCNTs/PPS/PA6 composite by the two-step blending method reached to 0.572W/(m K), which is 40.9% higher than that of composite by the one-step blending method. The reason for the improved thermal conductivity is the increased effective volume concentration of MWCNTs in single (PPS) phase. Especially, the DSC results and SEM observations showed that there were distinct differences in the crystallization and morphology of the samples prepared by the different mixing sequences. Moreover, a great influence on thermal conductivity and thermal stability of MWCNTs were found. The thermal conductivity of MWCNTs/PPS/PA6 composite with 36.36 wt % MWCNTs is 1.12 W/(m K), which is 331% enhancement compared to those of pure matrix based PPS/PA6 composites.

DOI: 10.1134/S1560090421060154

INTRODUCTION

Polymer-based thermal conductive composites have attracted a considerable research interest in polymer industry due to their superior properties such as light weight, insulation, corrosion resistance and easy processing [1–3]. At present, it is a common method to prepare most thermoplastic polymer thermal conductive composites by adding a great range of thermal conductive fillers into polymers with appropriate process, auxiliary agent and processing method [4–7].

Polymer blends can combine the properties of several polymer components and improve the comprehensive properties of materials [7–9]. In the study of thermal conductivity composite materials, the double percolation structure is used to elective localization of fillers in one phase of the co-continuous blends [10–13]. Such a strategy could effectively reduce the volume fraction of fillers while retaining high thermal conductivity. Al-Saleh et al. [14] studied carbon black (CB) filled polypropylene (PP)/ polystyrene (PS) polymer blends and a reduced percolation threshold was detected for the selective localization of CB at the interfaces of PP/PS blend. Zhou et al. [15] investigated graphite filled immiscible Polyamide 6 (PA6)/polypropylene (PP) blend and reached the conclusion that the thermal conductive properties of graphite-containing blend showed enhanced conductivity for the double-percolation structure compared with that of single polymer composites containing the same graphite loading.

Inspired by this, we investigated MWCNTs modified PPS/PPS immiscible blends to obtain thermal conductive materials. PA6 is a thermoplastic engineering plastic with good comprehensive performance and wide application [16–19]. However, the amide group leads to the shortcomings of nylon 6 in practical application, such as high water absorption and poor dimensional stability [13, 20, 21]. PPS has excellent comprehensive mechanical properties, heat resistance, chemical resistance, good dimensional stability and other advantages [22–24]. It also has a good affinity with inorganic substances [25]. MWCNTs were used as the functional filler to enhance the heat conduction properties of PPS/PA6 binary blends. But for one problem of easy agglomeration due to their small particles, large specific surface area, high specific surface energy and great interparticle interaction [26–30]. Therefore, in order to optimize their dispersion in the matrix, they should generally treated with surface modification in practical applications [31, 32].

The expection of this study is thermal conductive filler can disperse between PPS/PA6 in one phase to optimize the filler distribution and form thermal conductive paths, thus improving the thermal conductivity of the resultant composites. In this paper, the mor-

phology and properties such as thermal, DSC of the composites would be reported and discussed mainly based on the weight fraction of MWCNTs and preparation method.

EXPERIMENTAL

Materials

CNTs (purity, >95%; outer diameter, 30–50 nm; inside diameter, 5–12 nm; length, 10–20 μm) was purchased from Shenzheng Tulin Scientific And Technical Co., Ltd., China. (3-Glycidyloxypropyl)trimethoxysilane (KH560) was produced by Sinopharm Chemical Reagent Co., Ltd., China. 70% nitric acid and 95% sulfuric acid of analytical grade were obtained from Sinopharm Chemical Reagent Co., Ltd., China. Ethylene (E)-acrylate (MA)-glycidyl methacrylate (GMA) copolymer (Lotader Ax8900) was produced by French Arkema Co., Ltd., France. PA6(B3L) was supplied by BASF Co., Ltd., Germany. PPS (powder) was supplied by Guangzhou Jinfa Technology Co., Ltd., China.

MWCNTs Surface Treatment

Firstly, MWCNTs were dispersed in 70% concentrated nitric acid with assistance of ultra-sonication for 2 h to get a uniform suspension. The carbon nanotube suspension was then stirred by magnetic force and refluxed at 80°C for 6 h. The residual concentrated nitric acid in the suspension was washed out with concentrated hydrochloric acid, diluted and filtered repeatedly with deionized water until the PH of the solution was about 5, and then the modified carbon oxide nanotubes (O-MWCNTs) were obtained through extraction filtration. The O-MWCNTs were dried for 12 h at 120°C.

KH560 (1 wt % of filler) and ethanol (5 times the mass of KH560) were mixed evenly. Then MWCNTs were added to this mixture separately, mechanical stirring for 0.5 h, accompanied by ultrasonic dispersion, static processing. The fillers were obtained after vacuum drying at 80°C for 12 h.

Preparation of PA6/PPS/MWCNTs Composite

Melt mixing was carried out by a single screw extruder (SHJ-20, Nanjing Jaya extrusion Equipment Co. Ltd.). The poly(phenylene sulfide) (PPS) and polyamide 6 (PA6) were dried at 85°C for 12 h before mixing. In the two-step blending method, MWCNTs and PPS were melted to prepare the substrate, and then PA6 and e-MA-GMA, compatibilizer, were melted to blend with the substrate to obtain thermal conducting composites. One-step blending method is to prepare composites with the same filling amount by direct melting of MWCNTs, PPS, PA6 and compatibilizers. The extruding temperatures were set as 285, 280 and 270°C (from feeding section to extruding die), a screw rotation rate of 120 rpm. Later, the granules were placed in drying cabinet and dried at 85°C for 8 h, and test rectangle were prepared by vertical injection molding machine (XLB, Huzhou Shuangli Automatic Science and Technology Equipment Co., Ltd.).

Characterization

Fourier-transform infrared (FTIR). A small amount of carbon nanotube samples were dried and ground thoroughly with potassium bromide (KBr) powder. The samples were pressed into a sheet and placed on a Nicolet 6000 infrared spectrometer manufactured by Thermo Nicolet for infrared spectrum analysis using transmission mode. The scanning range was 500–4000 cm^{-1}, and the resolution was 4 cm^{-1}.

Thermal conductivity measurement. The planar thermal conductivity measurement of the composite was tested by a thermal laser analyzer LFA457 (NETZSCH, Germany) at a voltage of 1634 V according to ASTM E1461. The through-plane thermal conductivity at three points of each sample was tested separately. The model was corrected by the Capel pulse. The average of these represented the ultimate through-plane thermal conductivity of each sample. The prepared cylindrical sheet had a diameter of 12.5 mm and a thickness of 2.5 mm.

Morphological characterizations. The sample was brittlely broken with liquid nitrogen to form an experimental article, and gold was sprayed to increase the resolution. Observation of cross-section microscopic morphology used a scanning electron microscope (JSM-6363LV).

Differential scanning calorimetry (DSC). DSC1/JYH-86 differential scanning calorimetry analyzer was used to analyze the crystallization and melting behavior of the composite under nitrogen atmosphere (50 mL/min) protection. Among them, the sample mass is 8–10 mg and the test standard is ISO 11357-3-2011. Firstly, the sample was heated to 320°C at a speed of 30°C/min, and the heat was kept for 5 min to eliminate the history of heat. Then the sample was cooled to 25°C at a cooling rate of 10°C/min and kept for 10min to obtain the cooling crystallization curve. Finally, the sample was heated to 320°C at a heating rate of 10°C/min to obtain the heating melting curve.

Thermogravimetric analysis (TGA). The STA 449C comprehensive thermal analyzer was used to conduct thermogravimetric analysis and test on the composite

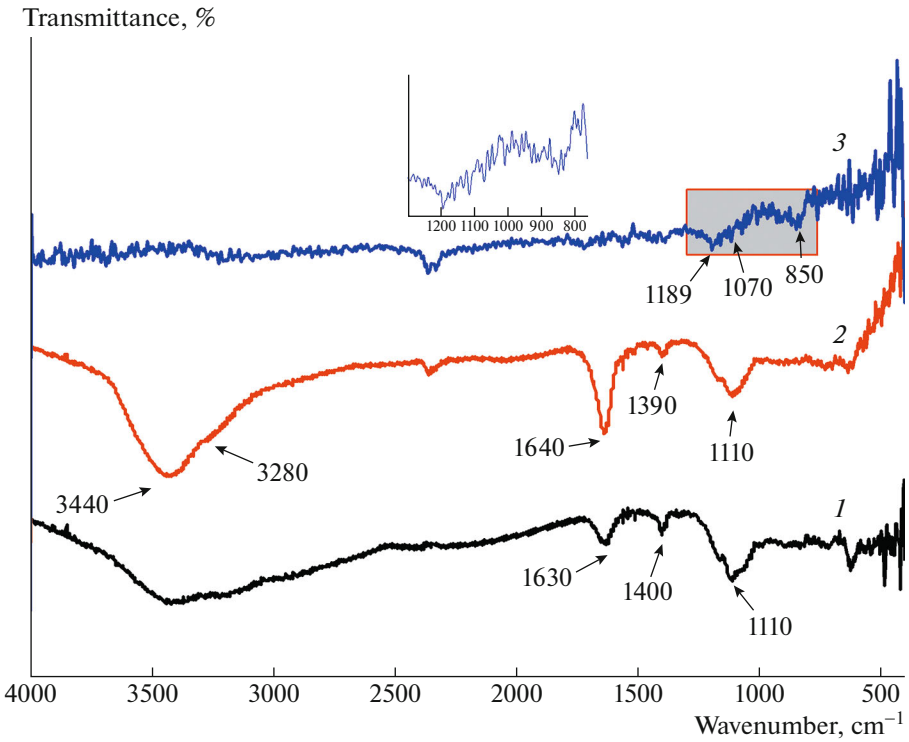

Fig. 1. FTIR spectra of (*1*) MWCNTs, (*2*) O-MWCNTs, and (*3*) MWCNTs-KH560.

material under the protection of argon atmosphere. The test temperature ranged from 30 to 400°C, and the heating rate was 10°C/min.

RESULTS AND DISCUSSION

Characteristics of Functionalized Filler

To enhance the affinity between the MWCNTs and matrix, MWCNTs was modified by KH560 silane agent. The FTIR spectra of original carbon nanotubes (MWCNTs), oxidized carbon nanotubes (O-MWCNTs), and carbon nanotubes modified by KH560 (MWCNTs-KH560) were plotted in Fig. 1. For original MWCNTs, a broad absorption band centered at 3440 cm^{-1} owes to the stretching vibration peak of O–H. For O-MWCNTs, compared with the original MWCNTs, the peak at 3750–3000 cm^{-1} was more obvious. In addition, the characteristic absorption peak of MWCNTs at 1630 cm^{-1} and O-MWCNTs at 1640 cm^{-1} was caused by the stretching vibration of C=O in carbonyl and carboxyl groups, and the peak became more obvious and sharper after acidification. In the case of MWCNTs-KH560, new absorption bands located at 850, 1070, and 1189 cm^{-1} appeared, which can be ascribed to the absorption bands of epoxy groups, Si–O–C, and O–C, respectively. These characteristic peaks proved that the MWCNTs particles have been grafted with KH560 silane coupling agent.

Figure 2 shows the dispersion of MWCNTs, O-MWCNTs and MWCNTs-KH560 with the same mass after ultrasonic dispersion in *n*-methylpyrrolidone (NMP) solvent for different standing time. According to Fig. 2a, it can be found that the MWCNTs are not evenly dispersed after ultrasonic dispersion for 20 min, but dispersed in the form of small pieces floating in the solvent. The modified O-MWCNTs and MWCNTs-KH560 were uniformly dispersed in the solvent, making the whole solution appear black. These results indicated that the O-MWCNTs grafted with oxygen-containing functional groups and the MWCNTs-KH560 modified with coupling agent showed good dispersion in NMP, were easily opened by ultrasonic oscillation, and had a strong intermolecular force with the strongly polar solvent. After standing for 24 h, only a small part of the original carbon nanotubes can be evenly dispersed in the NMP solvent, and most of the carbon nanotubes are deposited at the bottom of the bottle. However, O-MWCNTs and MWCNTs-KH560 were still evenly dispersed in the solvent, and no precipitation occurred. This indicates that the dispersion of carbon nanotubes in NMP is poor, while O-MWCNTs and MWCNTs-KH560 in NMP is good. The dispersion

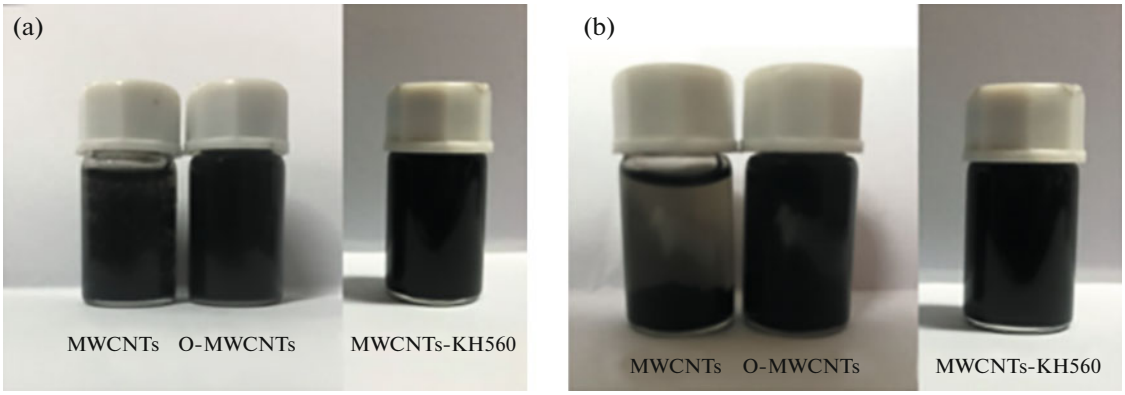

Fig. 2. MWCNTs and O-MWCNTs in NMP solvent after (a) ultrasonic dispersion treatment for 20 min, (b) standing for 24 h.

test showed that the modification of MWCNTs did improve the dispersion of the filler.

Effect of Melt Blending Sequence on Composites

Morphology. The morphology of the cryo-fractured surface of the composites, which prepared by different melt blending sequence, is shown in Fig. 3. Photo 3a shows that the accumulation density of MWCNTs was low and the filler did not form a continuous phase in the matrix. Photos 3b and 3c show that the contrast between the light and dark regions is different, and EDS analysis also observed that the sulfur content in the light and dark regions is quite different (Table 1). Combined with photo 3b and Table 1, it can be seen that MWCNTs were concentrated and dispersed in high brightness regions. The sulfur content in the bright area is high, and the sulfur content in the dark area is obviously low. Therefore, it was inferred that the bright region of this cross section was mainly the PPS phase and the dark region was mainly the PA6 phase. The EDS spectrum indicates that MWCNTs prepared by two-step blending method are mainly dispersed in PPS phase. Photo 3d microstructure shows that the "banded" biphasic continuous structure is preliminarily formed in composite materials. The E-MA-GMA acts as a bridge, which increases the compatibility of the two phases. The molecular chains of PPS and PA6 contact with each other, piling up and interpenetrating each other, which transforming the blend system from a "sea-island" structure with high surface tension to a two-phase continuous structure with low tension "silk ribbon".

Table 1. EDS data of MWCNTs/PPS/PA6 two-step blending system

Element	Mass percent, wt %	
	Spot 1	Spot 2
C	69.16	67.42
N	0.48	8.34
O	3.10	16.3
S	27.25	7.93

Fig. 3c: energy spectrum data at each point of the cross-section of MWCNTs/PPS/PA6 composite.

Thermal conductivity. Table 2 shows the thermal conductivity of the composite prepared by the two processes. It can be seen that the composite prepared by two-step blending shows higher thermal conductivity, which compared with direct melt blending. It should be noted that the increase of thermal conductivity with MWCNTs loading shows a faster growth tendency for composite prepared by two-step blending than that prepared by one-step blending. At MWCNTs loading of 8.69 wt %, the thermal conductivity of the two-step blend system is 0.572 W/(m K), which is 40.9% higher than that of the one-step blend and 116.7% higher than that of the matrix PPS/PA6. It can mainly be ascribed to the filler dispersed in different substrates during two preparation method. In the two-step blending, MWCNTs were mostly dispersed in the PPS phase, which accounted for 40 wt % in the whole matrix. In this case, MWCNTs forms denser networks of heat transportation. Therefore, the two-step blending could effectively increase the density of our prepared

Table 2. Thermal conductivity of MWCNTs/PPS/PA6 composites under different process conditions

Weight fraction of MWCNTs, wt %	One-step blending method, W/(m K)	Two-step blending method, W/(m K)
0	0.264	0.264
4.06	0.332	0.373
8.69	0.406	0.572

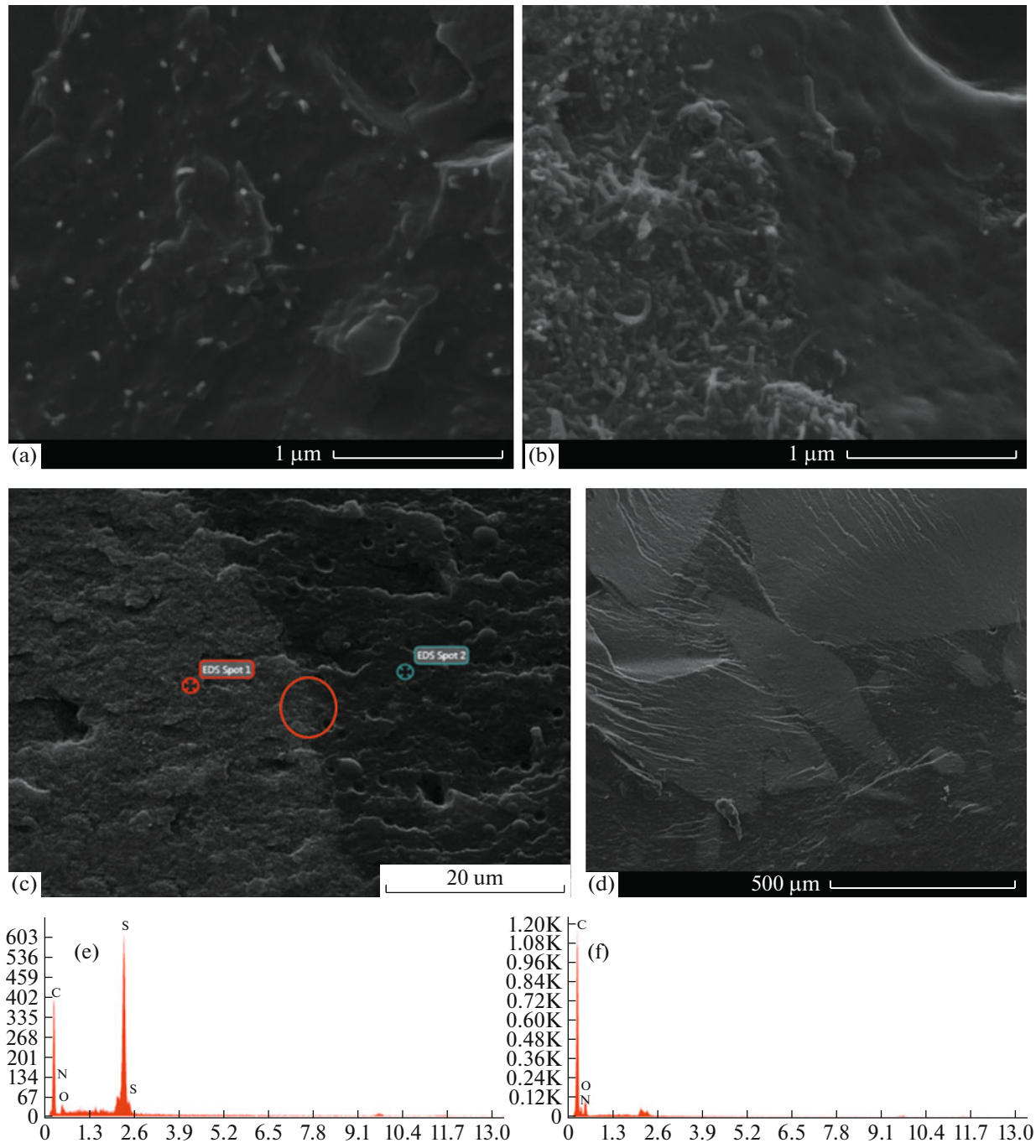

Fig. 3. SEM photograph and EDS spectrum of MWCNTs/PPS/PA6 composite material. (a) One-step blended composite material with MWCNTs content of 8.69 wt %; (b) two-step blended composite material with MWCNTs content of 14.04 wt % (high magnification); (c) two-step blended composite material with a MWCNTs content of 14.04 wt %; (d) two-step blended composite material with a MWCNTs content of 14.04 wt % (low magnification); (e, f) EDS spectrum correspond to (c) Spot1, Spot2.

composites, which enabled the densification of a thermally conductive network in the composites.

DSC measurements. Figure 4 shows the cooling crystallization and heating melting curves of the composite obtained by DSC testing. For clarity, all DSC scan curves shown here are shifted vertically. Table 3 lists the specific curve data. From the crystallization curve, the corresponding peak of PA6 phase and PPS phase around 185 and 240°C can be observed. There is no obvious correlation between PPS crystallization temperature peak value and process method (≤1°C), but there is difference in melt enthalpy. Melting

Table 3. Melting temperature, crystallization temperature and melting enthalpy of MWCNTs/PPS/PA6 blend system

Preparation technology	PPS			PA6		
	T_m, °C	T_p, °C	ΔH_f, J g^{-1}	T_m, °C	T_p, °C	ΔH_f, J g^{-1}
PPS/PA6	283.74	244.55	15.01	220.17	189.28	33.14
One-step blending	283.54	244.13	15.58	215.29	186.29	24.3
Two-step blending	283.42	243.96	11.61	218.70	189.56	31.66

Table 4. EDS data of the composite material with MWCNTs content of 20.25 wt %

Element	Mass percent, wt %	
	Spot 1	Spot 2
C	69.8	65.63
N	7.44	0.64
O	17.47	4.74
S	5.29	29.1

Fig. 5c: energy spectrum data at each point of the cross-section of composite.

Table 5. EDS data of the composite material with MWCNTs content of 27.59 wt %

Element	Mass percent, wt %	
	Spot 1	Spot 2
C	68.76	80.99
N	1.03	3.99
O	4.31	8.99
S	25.9	6.03

Fig. 6a: energy spectrum data at each point of the cross-section of composite.

enthalpy is proportional to crystallinity. It is found from Table 2 that the melting enthalpy of two-step blending PPS is 11.61 J g^{-1}, and that of one-step blending PPS is 15.58 J g^{-1}. Because the two-step blending packing is concentrated and dispersed in the PPS phase, MWCNTs, as nucleating agent, have reached the saturation value, which hinders the movement of PPS chain segment and leads to the decrease of crystallinity. In the two-step blending method, the crystallization temperature of PA6 phase was 189.56°C, and that of one-step blending was 186.29°C. The crystallization peak and initial crystallization temperature of PA6 phase obviously moved towards high temperature. This indicates that in one-step blending, the fillers are uniformly dispersed in PPS phase and PA6 phase, the MWCNTs have a strong heterogeneous nucleation effect on PA6by this time. Observing the DSC second-heating curves (Fig. 4b) and Table 3, it is clearly seen that the melting point of PPS was not significantly changed in the two processes. The melting point of PA6 decreased with the addition of fillers, and the one-step blending system decreased by 5°C, which showed an obvious decrease.

Effect of Carbon Nanotube Content on Composites

Since the two-step blending method can improve the thermal conductivity of materials, the following experimental samples are prepared by two-step blending.

Morphology. The morphology of the cryo-fractured surface of the composites is shown in Figs. 5 and 6. The picture demonstrates an incremental mass ratio of MWCNTs in the matrix from 8.69 wt % to 27.59 wt %. Tables 4 and 5 correspond to major EDS data. As can be seen from the SEM figure, when the content of MWCNTs is 8.69 wt %, MWCNTs were distributed in an "island" shape in the composite material and were not able to connect each other into a heat conduction network, leading to the low thermal conductivity. Photo 5b shows that carbon nanotubes are concentrated in PPS phase and gradually form a continuous phase. Photos 5c and 5d indicate that the interface between PPS and PA6 phases is gradually blurred, and a small amount of MWCNTs migrate and disperse in PA6 phase. Specifically, at MWCNTs loading of 27.58 wt %, fillers appeared obviously in PA6 phase, indicating that part of MWCNTs migrated to PA6 phase during melt blending, as shown in Fig. 6. The SEM photography manifests that the higher filling amount was, the less positioning effect of two-step melt blending process on the filler was, and the filler tended to be uniformly distributed in the whole PPS/PA6 matrix.

Thermal conductivity. The thermal conductivity values of MWCNTs/PPS/PA6 blends with different filler content are shown in Fig. 7, it can be seen that thermal conductivity increased obviously with the increasing of filler loadings. The maximum thermal conductivity of 1.12 W/(m K) was obtained in MWCNTs/PPS/PA6 composite filled with 36.36 wt % fillers, which is 4.31 times higher than pure PPS/PA6 blend. This is attributed to the formation of densely packed heat conduction network throughout

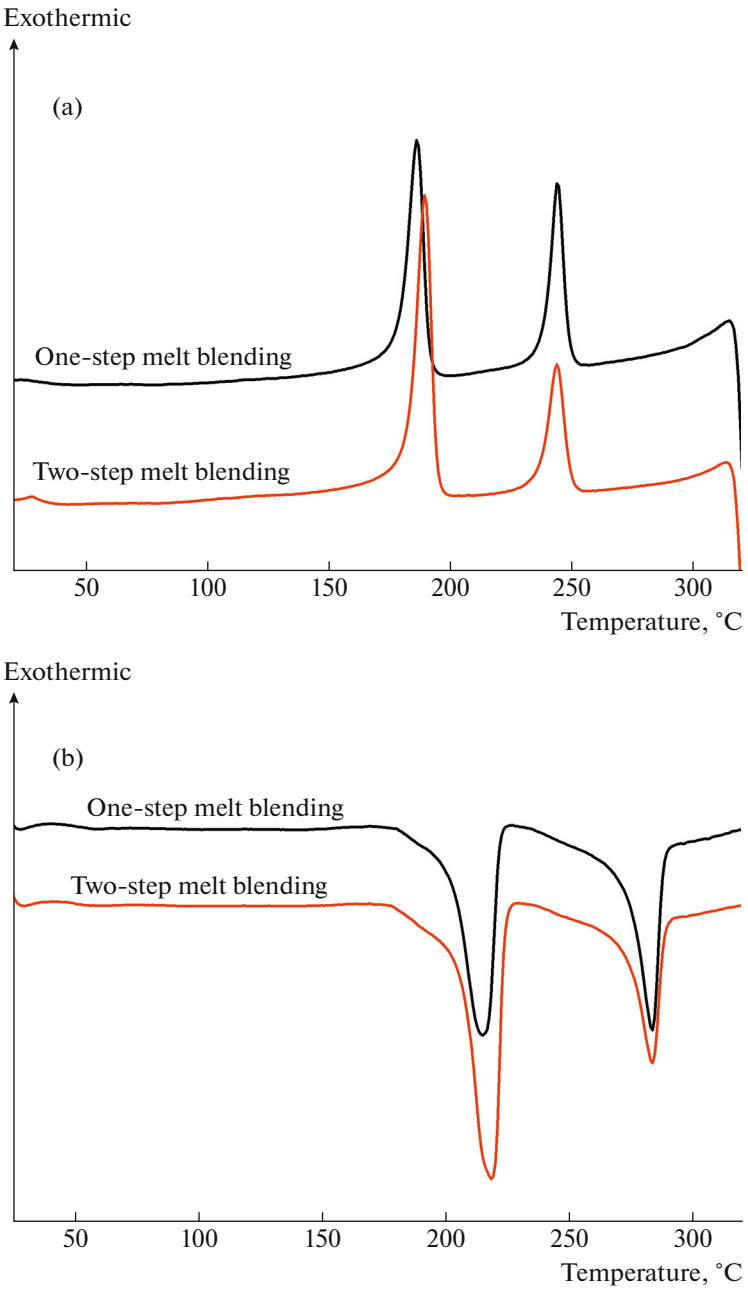

Fig. 4. (a) DSC cooling curves obtained from MWCNTs/PPS/PA6 blends by different processes and (b) DSC second-heating curves obtained from MWCNTs/PPS/PA6 blends by different processes.

the composite. It was found that the thermal conductivity of the composite material did not climb sharply with the increase of carbon nanotubes filling amount, and the slope amplitude gradually decreased. This is due to the fact that phonons scatter heavily at the interface. Therefore, as the content of MWCNTs in the matrix increased, the interfacial defects increased, which affected the phonon transfer and generated huge interfacial thermal resistance, reducing the increase of thermal conductivity of MWCNTs/PPS/PA6 composites.

DSC measurements. Figure 8 shows the DSC cooling crystallization and heating melting curves of the composites with different carbon nanotube filling volumes. The melting temperature (T_m) corresponding to the melting absorption peak of PA6 is about 220°C, which can be obviously observed in the DSC melting curve. The T_m corresponding to the melting absorption peak of PPS is about 283°C, and PPS and PA6 are incompatible. T_m and crystallization peak temperature (T_p) of PPS phase decreased significantly with the

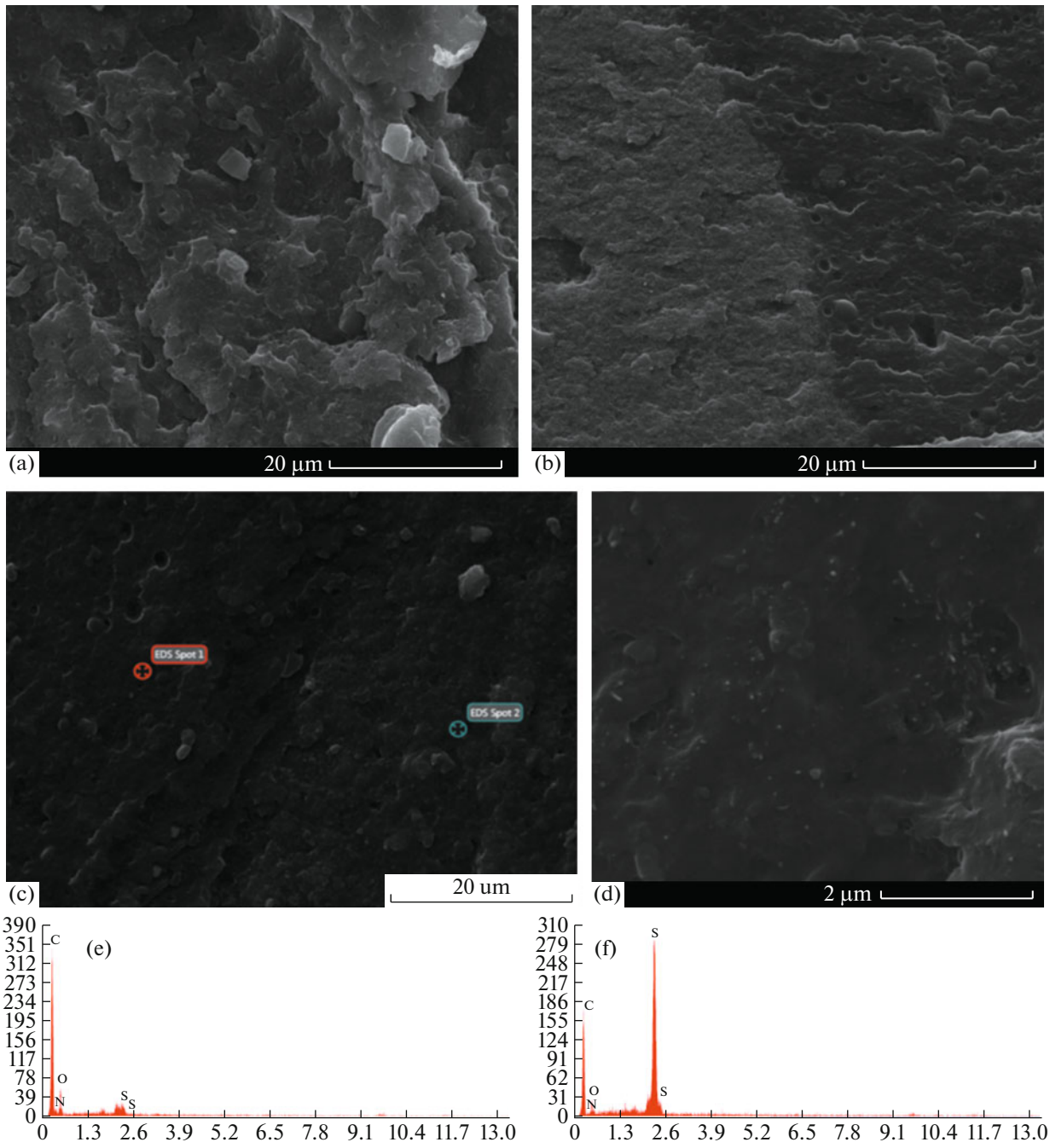

Fig. 5. SEM images of MWCNTs/PPS/PA6 composite materials: the corresponding carbon nanotube filling amounts are (a) 8.69, (b) 14.04, and (c) 20.25 wt %; (d) is a partially enlarged view of (c); (e, f) EDS spectrum corresponds to (c) Spot 1, Spot 2.

increase of filling volume. It can be ascribed to the MWCNTs in the matrix as they blocked the entangled connection of molecular chain segments. In addition, the increase in the content of MWCNTs resulted in the broadening of T_m peak pattern, which also indicated the limitation of PPS chain movement. And it also can be seen from Table 6 that the melting enthalpy of PPS phase also decreases significantly. It can be ascribed to the fact that the higher the filling amount is, the greater the restriction of PPS molecular chain get.

The distribution of fillers in the blend system can also be observed from DSC atlas. When the filling amount was low, the content of MWCNTs had no

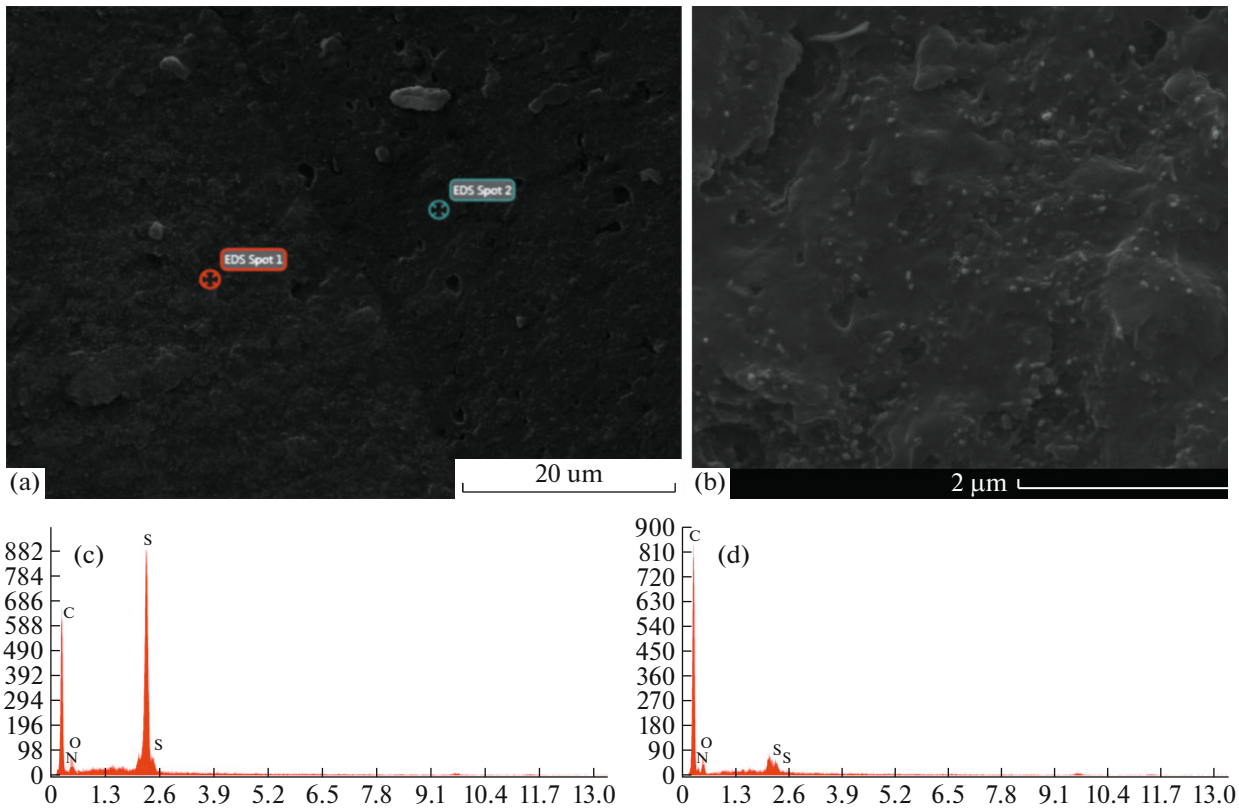

Fig. 6. (a) SEM image of MWCNTs/PPS/PA6 composite material with 27.59 wt % carbon nanotube filling content; (b) partially enlarged SEM image of the composite material cross section; EDS spectra (c, d) correspond to (a) Spot 1, Spot 2, respectively.

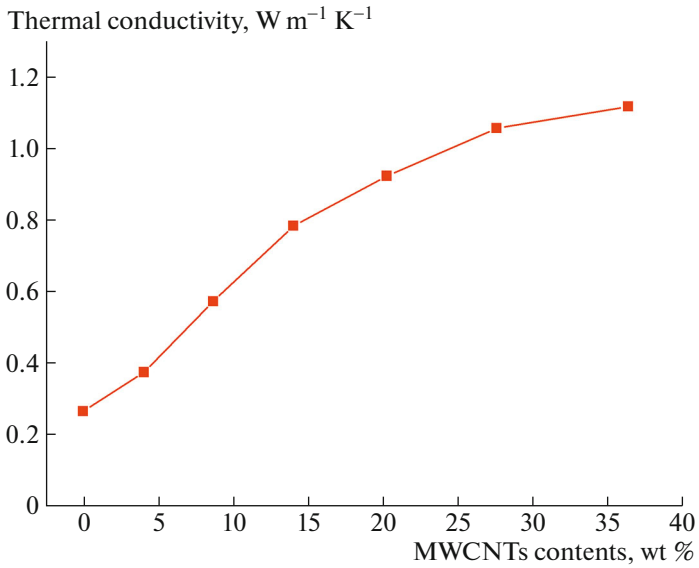

Fig. 7. Thermal conductivity of MWCNTs/PPS/PA6 composites at different MWCNTs content.

significant effect on the T_m and T_p of PA6 phase, indicating that MWCNTs were mainly concentrated and dispersed in PPS phase. At this time, the dispersion difference of PPS substrate in PA6 phase resulted in slight changes in the melting point and crystallization temperature of PA6 phase. At the

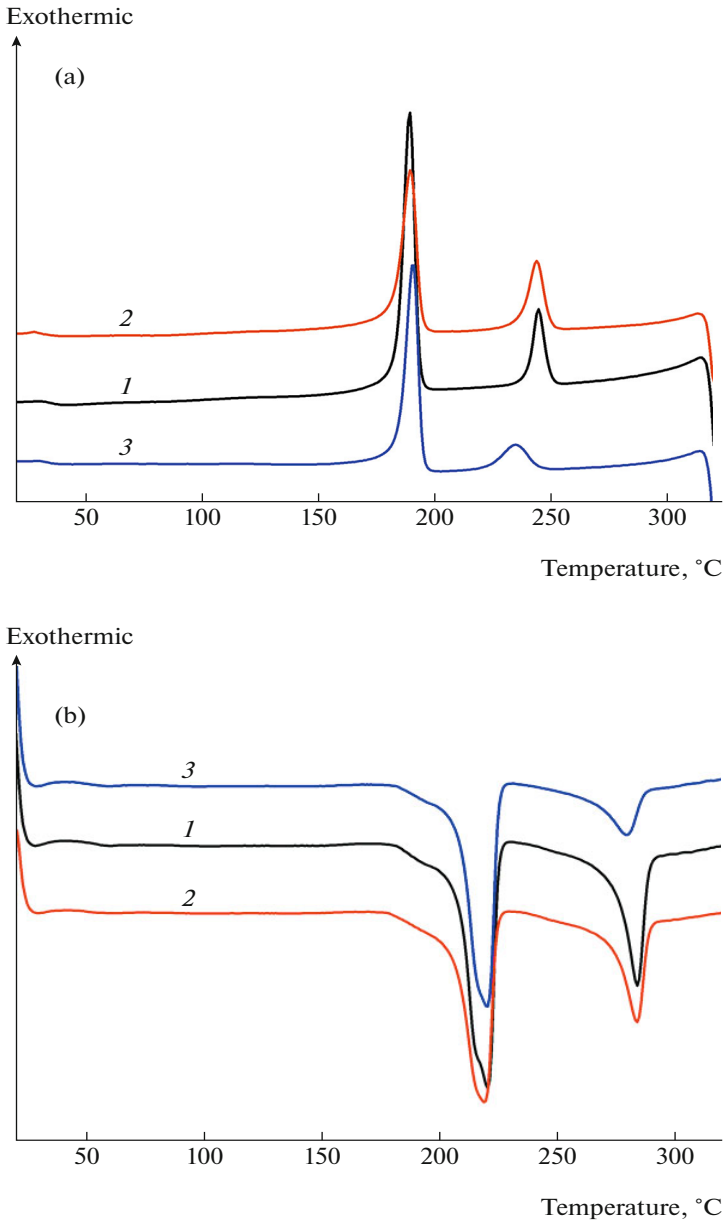

Fig. 8. (a) DSC cooling curves obtained from MWCNTs/PPS/PA6 blends and (b) DSC second-heating curves obtained from MWCNTs/PPS/PA6 blends. (*1*) PPS/PA6, (*2*) 8.69 wt % MWCNTs/PPS/PA6, and (*3*) 20.25 wt % MWCNTs/PPS/PA6.

MWCNTs loading fraction of 20.25 wt %, the crystallization temperature and melting point of PA6 phase increased slightly. At this time, a small amount of filler migrated and dispersed to PA6 phase, which played the role of heterogeneous nucleation and promoted crystallization, to some extent, resulting in much higher crystallinity for the high loading systems.

Thermogravimetric measurements. The TGA curves of all the samples under nitrogen atmosphere are shown in Fig. 9. It is obviously seen that the thermal stability of composites improves with the increase of filling amount. At the MWCNTs loading fraction of 8.69 wt %, the temperature of $T_{5\%}$ of the composite was increased but not significantly. At the MWCNTs loading fraction of 20.25 wt %, the $T_{5\%}$ of the composite material reaches 388.9°C, which is 13.9°C higher than the pure PPS/PA6. It comes down to: MWCNTs have good thermal stability, but when MWCNTs were dispersed phase in the PPS matrix exists at low filling volume, its thermal stability is not apparent. If the filling amount increased continuously, the filler will form a reticule-chain skeleton in the matrix, so that the thermal stability of

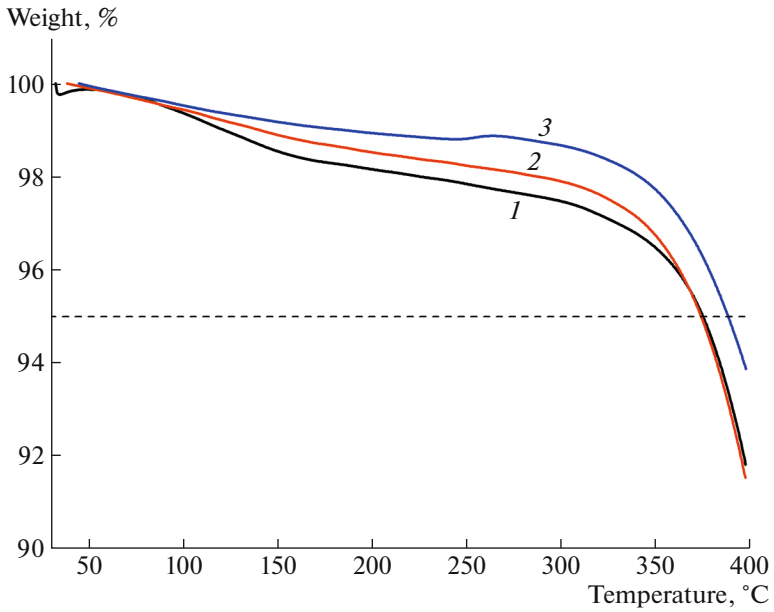

Fig. 9. TGA curves of composite materials with different carbon nanotube content: (*1*) PPS/PA6, (*2*) 8.69 wt % MWCNTs/PPS/PA6, and (*3*) 20.25 wt % MWCNTs/PPS/PA6.

Table 6. Melting temperature, crystallization temperature and melting enthalpy of MWCNTs/PPS/PA6 blend system under different loadings

Weight fraction of MWCNTs, wt %	PPS			PA6		
	T_m, °C	T_p, °C	ΔH_f, J g^{-1}	T_m, °C	T_p, °C	ΔH_f, J g^{-1}
0	283.74	244.55	15.01	220.17	189.28	33.14
8.69	283.42	243.96	11.61	218.70	189.56	31.66
20.25	278.90	234.68	6.41	219.94	190.64	32.76

MWCNTs is shown. Moreover, a small amount of MWCNTs migrating to PA6 phase improved the thermal stability of PA6 phase, thus affecting the thermal stability of the composite.

CONCLUSIONS

The MWCNTs modified PPS/PA6 blend composites were obtained by melt blending process. Compared with the one-step blending method, the composite prepared by two-step blending showed higher thermal conductivity. The concept of effective volume concentration of MWCNTs is used to explain the dramatically improved thermal conductivity when using PA6/PPS 6 : 4 blend as the matrix.

On one hand, thermal conductivity increased with an increase in MWCNTs loading fraction. A high thermal conductivity of 1.12 W/(m K) was achieved at 36.36 wt % MWCNTs, which is 4.31 times higher than that of pure PA6/PPS blend. The results revealed the formation of thermal conductive paths is crucial to the enhancement of heat conduction ability for the MWCNTs filled composites. On the other hand, the MWCNTs act as protective agent and inhibited the decomposition of the PA6-PPS copolymer. At MWCNTs loading of 20.25 wt %, the $T_{5\%}$ of the composites reached 388.9°C, which was 13.9°C higher than that of pure matrix, showing good thermal stability.

ACKNOWLEDGMENTS

This work was financially supported by the Key Research and Development Project of Hunan Province (Grant no. 2018GK2063).

CONFLICT OF INTEREST

The authors declare that they have no conflicts of interest.

REFERENCES

1. J. G. Kovacs and A. Suplicz, J. Reinf. Plast. Compos. **32**, 16 (2013).

2. P. Bujard, G. Kuhnlein, S. Ino, and T. Shiobara, IEEE Trans. Compon., Packag., Manuf. Technol., Part A **17**, 4 (1994).
3. A.F. Osman and M. Mariatti, Polym. Polym. Compos. **14**, 6 (2006).
4. H. V. Madhad and D. V. Vasava, J. Thermoplast. Compos. Mater. (2019). https://doi.org/10.1177/0892705719880942
5. J. Xing, N. Fu, H. Ding, Z. Nan, and C. Tang, RSC Adv. **5**, 27 (2015).
6. S. Shen, A. Henry, J. Tong, R. Zheng, and G. Chen, Nat. Nanotechnol. **5**, 4 (2010).
7. J. J. Elmendorp and R. J. Maalcke, Polym. Eng. Sci. **26**, 6 (2010).
8. F. Wei, X. Fan, H. Q. Jiao, Z. W. Jin, and Y. Wei, Polym. Sci., Ser. A **61**, 6 (2019).
9. Y. Malekzadeh, K. Shelesh-Nezhad, and A. R. Adli, Polym. Sci., Ser. A **58**, 996 (2016).
10. J. P. Cao, X. Zhao, J. Zhao, J. W. Zha, G. H. Hu, and Z. M. Dang, ASC Appl. Mater. Interfaces **5**, 15 (2013).
11. F. Gubbels, R. Jerome, E. Vanlathem, R. Deltour, and F. Brouers, Chem. Mater. **10**, 5 (1998).
12. C. Zhang, X. S. Yi, H. Yui, S. Asai, and M. Sumita, Mater. Lett. **36**, 1 (1998).
13. S. Zhou, Y. Chen, H. Zou, and M. Liang, Thermochim. Acta **566**, 84 (2013).
14. M. H. Al-Saleh and U. Sundararaj, Composites, Part A **39**, 2 (2008).
15. S. Zhou, W. Luo, H. Zou, M. Liang, and S. Li, J. Compos. Mater. **50**, 3 (2016).
16. X. Fu, C. Yao, and G. Yang, Cheminform **46**, 37 (2015).
17. M. Li, H. Cui, Q. Li, and Q. Zhang, J. Reinf. Plast. Compos. **35**, 435 (2016).
18. C. Wang, H. Feng, K. Yang, T. Hu, W. Wang, R. Deng, Q. Jiang, and H. Zhang, RSC Adv. **6**, 51 (2016).
19. H. G. Xu, H. D. Zhou, X. D. Chen, and Y. F. Liu, Polym. Sci., Ser. A **57**, 644 (2015).
20. W. Yu, H. Xie, L. Yin, J. Zhao, L. Xia, and L. Chen, Int. J. Therm. Sci. **91**, 76 (2015).
21. M. Li, Y. Wan, Z. Gao, G. Xiong, X. Wang, C. Wan, and H. Luo, Mater. Des. **51**, 5 (2013).
22. Z. Hao, N. Ning, R. Su, Z. Qin, and F. Qiang, J. Appl. Polym. Sci. **106**, 4 (2010).
23. H. T. Oyama, M. Matsushita, and M. Furuta, Polym. J. **43**, 12 (2011).
24. T. Yin, Y. Q. Gu, J. H. Gao, and W. Y. Yu, Adv. Mater. Res. **804**, 98 (2013).
25. P. J. Yoon and J. L. White, J. Appl. Polym. Sci. **51**, 8 (1994).
26. M. Abu-Abdeen, O. Saber, J. Mazher, M. M. Ahmed, and M. Gouda, J. Thermoplast. Compos. Mater. **33**, 1499 (2020).
27. S. B. Sinnott and R. Andrews, CRC Crit. Rev. Solid State **26**, 3 (2001).
28. Z. Han and A. Fina, Prog. Polym. Sci. **36**, 7 (2011).
29. L. Lin, Y. T. Han, X. H. Zhao, Y. W. Wang, H. B. Zhang, Z. H. Jiang, and Z. Chen, High Perform. Polym. **31**, 875 (2018).
30. X. Zhang, H. Xiang, X. Li, X. Wen, and C. Lu, Polym. Sci., Ser. A **61**, 6 (2019).
31. N. Song, J. Yang, P. Ding, S. Tang, and L. Shi, Composites, Part A **73**, 232 (2015).
32. S. Bose, R. A. Khare, and P. Moldenaers, Polymer **51**, 5 (2010).